JOURNAL OF THERMOPHYSICS AND HEAT TRANSFER
Vol. 22, No. 1, January–March 2008

Radiative Gas Dynamic Model of Hydrogen Laser-Supported Plasma Generator

S. T. Surzhikov
Institute for Problems in Mechanics Russian Academy of Sciences, Moscow, Russia
and
M. Capitelli, G. Colonna, and C. Gorse
University of Bari,
Istituto di Metodologie Inorganiche e dei Plasmi-Consiglio Nazionale delle Ricerche, Bari, Italy

DOI: 10.2514/1.29982

Radiative gas dynamics of a hydrogen laser-supported plasma generator and radiative heating of the internal surface of the plasma generator are studied numerically. For this purpose, a radiative gas dynamic model of the laser-supported wave in the cylindrical channel of the laser-supported plasma generator is created. The model is based on the Navier–Stokes equations, energy conservation equation for heat conducting gas in chemical equilibrium, and the radiation heat transfer equation using the multigroup spectral approximation. The numerical study is performed for the typical parameters of the laser-supported plasma generator: input velocities $u_0 = 10$–200 m/s, pressure $p = 1$ atm, and CW CO_2 laser radiation power $P_L = 100$–200 kW.

Nomenclature

B_ν	=	the Planck intensity
c	=	speed of light
c_p	=	specific heat at constant pressure
h	=	the Planck constant
J_ν	=	spectral intensity
k	=	the Boltzmann constant
L_c	=	length of LSPG chamber
NI	=	number of grid nodes in radial direction
NJ	=	number of grid nodes in axial direction
NS	=	number of grid nodes along ray
N_g	=	number of spectral group
N_φ	=	number of rays for azimuth direction
N_θ	=	number of rays for latitudinal direction
P_L	=	power of laser radiation
p	=	pressure
Q_{HR}	=	power of heat release because of thermal radiation
Q_L	=	power of heat release because of absorption of laser radiation
R_b	=	radial boundary of laser beam
R_c	=	radius of LSPG chamber
$\boldsymbol{R}_j$	=	radius vector of jth point on surface in laboratory coordinates
R_0	=	universal gas constant
r	=	radial coordinates
s	=	distance along ray
T	=	temperature
T_w	=	surface temperature
t	=	time
U	=	medium radiation density
U_b	=	black body radiation density
u	=	axial velocity
u_0	=	axial entrance velocity
$\boldsymbol{V}$	=	velocity
v	=	radial velocity
W_ν	=	density of spectral radiation energy
W_Σ	=	molecular weight of gas mixture
x	=	axial coordinates
x_f	=	axial coordinate of focused laser radiation
$\Delta\omega$	=	spectral region
ε	=	auxiliary function for interpretation of derivative of density in time domain
θ	=	azimuthal angle
κ	=	group absorption coefficient of thermal radiation
λ	=	conductivity
μ	=	viscosity
μ_ω	=	absorption coefficient for laser radiation
ρ	=	density
τ_ν	=	spectral optical depth
φ	=	azimuthal angle
ω	=	vortex function
ψ	=	stream function
$\boldsymbol{\Omega}$	=	unit vector of radiation heat transfer propagation

Subscripts

g	=	spectral group
i, j, k, l	=	spatial indexes in marching directions
m, n	=	spatial indexes in angular directions
w	=	wall condition
θ	=	latitudinal direction
ν	=	spectral characteristics
φ	=	azimuthal direction
ω	=	laser radiation wave number

I. Introduction

A STEADY-STATE plasma in a laser-supported plasma generator (LSPG) is maintained by continuous laser radiation, usually from a CW CO_2 laser, as the laser intensities sufficiently low to avoid optical breakdown [1]. There are generally three techniques used to produce laser-supported waves (LSWs), and all of them require some initial ionization to facilitate plasma formation. This may be done using an electric discharge or a source of ionizing radiation, or the laser beam itself can be used by irradiating a solid target and creating some ionization near the target surface by thermal ionization of the vaporized target material.

In addition to their scientific interest, the laser-supported waves (LSWs) phenomena are important for several reasons involving the practical applications of laser technology and plasma aerodynamics.

Presented as Paper 0638 at the 40th AIAA Aerospace Sciences Meeting and Exhibit, Reno, NV, 14–17 January 2002; received 24 January 2007; revision received 8 September 2007; accepted for publication 11 September 2007.

For example, the LSW can provide stable, localized, stationary plasmas in a number of gases over a wide range of pressure. Since the plasma temperatures are high compared with other kinds of discharges ($T \sim 20,000$ K), laser-supported plasma can be useful for spectroscopic and other kinds of investigations that require intense sources of radiation, particularly in the ultraviolet. The LSWs phenomena frequently arise during material processing, such as welding and cutting, in which high laser intensities are used. Because these phenomena drastically change the nature of the radiation incident on the working surface, special procedures are sometimes required to prevent their formation.

Another possible application of these phenomena in the field of space vehicle propulsion is the laser thrusters. This concept involves the generation of LSWs in a suitable working gas (hydrogen is most effective for these purposes) in a combustion chamber, with subsequent expansion of the heated gas through a supersonic nozzle. Such thrusters, theoretically capable of producing a very high specific impulse, have been studied both theoretically and experimentally in the last decade.

There are many papers dedicated to experimental and theoretical studies of the laser-supported waves, laser plasma generators, and laser-supported rocket engines. We will refer to some of them. The concept of the laser-supported rocket propulsion is discussed in [2,3]. Experimental study of the LSW in the radiative mode is described in [4–7]. Various kinds of numerical simulation models are presented in [8–15]. A nonequilibrium model of hydrogen LSPG is created in [16] for thermoconductive modes.

A general peculiarity of the present study is the numerical analysis of the radiative mode of a hydrogen LSPG. A spatial dimension of the LSW is so large (actually, this dimension is fixed by the radius of the laser beam) that the heat conductive mode of the LSWs' existence is changed into a radiative one. In other words, in the case under consideration, there are two general energy transfer mechanisms providing the LSW existence: absorption of the laser radiation and radiation heat transfer of the LSW with the ambient atmosphere. The case of the thermal conduction mode was studied in earlier publications [16–19].

Unfortunately, until the present, there is no evidence of creation of an LSPG functioning in a radiative mode. Therefore, numerical simulation results presented in the present paper are largely prognostic. To increase the reliability of the numerical simulation results, the computing code and integrated databases of thermophysical and optical properties were repeatedly tested on the examples available experimentally and from calculation data from other authors. Namely, the radiative gas dynamic calculations were tested and compared with experimental data [6,7,20] on the dynamics of laser-supported waves in the immovable atmosphere and in countercurrent, parallel, and cross flows of air [7,21,22]. Finally, the numerical simulation code tested the thermal gravitation convection around a continuous optical discharge inside a closed cylindrical chamber [23,24]. As far as the reliability of thermophysical and spectral optical properties used in this model, they were tested many times in our previous papers [25,26].

II. Radiative Gas Dynamics of the Laser Supported Plasma Generator

The geometry of the LSPG is shown in Fig. 1. The plasma generator is represented by a cylindrical chamber, in which the laser plasma is created at some distance x_f (the focal point of laser radiation) from the entrance.

The laser radiation flux (in this case a CW CO_2 laser with a wavelength $\lambda = 10.6$ μm) is sufficient for maintaining the plasma in the laser radiation field without inducing breakdown. The characteristic sizes of the laser plasma are determined by transversal sizes of the laser beam R_b in that place in which the plasma is localized. Velocities of the gas inside the LSPG channel are subsonic ($\sim$10–200 m/s), but temperatures achieve magnitudes of $\sim$15,000–20,000 K. High temperatures of the LSW require a description of the coupled gas dynamic and radiation processes inside such laser-supported waves and a prediction of the radiative

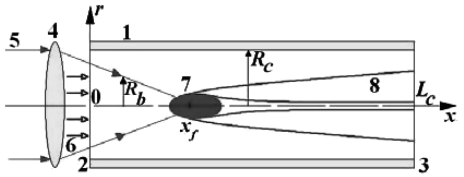

Fig. 1 Schematic of the LSPG. 1) cylindrical chamber of the LSPG; 2) inflow face of the chamber; 3) outflow face of the chamber; 4) focusing lens; 5) laser beam; 6) input gas stream; 7) laser-supported wave; 8) plume of the laser plasma; R_c=radius of inner surface of the chamber; calculation domain is bounded by $x \in [0, L_c]$ and $r \in [0, R_c]$.

heating of the LSPG internal surfaces. Creation of a computational model for describing such a coupling in gas and plasma flows is the main goal of the present study.

The radiative gas dynamic model of the LSPG in a two-dimensional cylindrical domain is composed of the following equations:

$$\frac{\partial \rho}{\partial t} + \frac{\partial(\rho u)}{\partial x} + \frac{1}{r}\frac{\partial(r\rho v)}{\partial r} = 0 \tag{1}$$

$$\rho\left(\frac{\partial u}{\partial t} + u\frac{\partial u}{\partial x} + v\frac{\partial u}{\partial r}\right) = -\frac{\partial p}{\partial x} + \frac{4}{3}\frac{\partial}{\partial x}\left(\mu\frac{\partial u}{\partial x}\right) + \frac{1}{r}\frac{\partial}{\partial r}\left(r\mu\frac{\partial u}{\partial r}\right) + \frac{1}{r}\frac{\partial}{\partial r}\left(r\mu\frac{\partial v}{\partial x}\right) - \frac{2}{3r}\frac{\partial}{\partial x}\left(\mu\frac{\partial rv}{\partial r}\right) \tag{2}$$

$$\rho\left(\frac{\partial v}{\partial t} + u\frac{\partial v}{\partial x} + v\frac{\partial v}{\partial r}\right) = -\frac{\partial p}{\partial r} + \frac{\partial}{\partial x}\left(\mu\frac{\partial u}{\partial r}\right) + \frac{\partial}{\partial x}\left(\mu\frac{\partial v}{\partial x}\right) + \frac{4}{3r}\frac{\partial}{\partial r}\left(r\mu\frac{\partial v}{\partial r}\right) - 2\frac{\mu v}{r^2} - \frac{2}{3}\frac{1}{r}\frac{\partial}{\partial r}\left(r\mu\frac{\partial u}{\partial x}\right) - \frac{2}{3}\frac{1}{r}\frac{\partial \mu v}{\partial r} + \frac{2}{3}\frac{\mu}{r}\left(\frac{\partial u}{\partial x} + \frac{1}{2}\frac{\partial(rv)}{\partial r}\right) \tag{3}$$

$$\rho c_p\left(\frac{\partial T}{\partial t} + u\frac{\partial T}{\partial x} + v\frac{\partial T}{\partial r}\right) = \frac{\partial}{\partial x}\left(\lambda\frac{\partial T}{\partial x}\right) + \frac{1}{r}\frac{\partial}{\partial r}\left(r\lambda\frac{\partial T}{\partial r}\right) + Q_L - Q_{\mathrm{HR}} \tag{4}$$

$$Q_L = \frac{\mu_\omega P_L}{\pi R_b^2}\exp\left(-\frac{r^2}{R_b^2}\right) \tag{5}$$

$$\frac{\partial P_L}{\partial x} = -\mu_\omega(x, r=0)P_L \tag{6}$$

$$Q_{\mathrm{HR}} = \sum_{g=1}^{N_g} \kappa_g(U_{b,g} - U_g)\Delta\omega_g \tag{7}$$

$$\mathrm{div}\left(\frac{1}{3\kappa_g}\mathrm{grad}U_g\right) = -\kappa_g(U_{b,g} - U_g), \qquad g = 1, 2, \ldots, N_g \tag{8}$$

where u and v are the projections of the flow velocity v on the x and r axes; ρ, p, c_p, μ, and λ are the density, pressure, specific heat at constant pressure, viscosity, and thermal conductivity, respectively; T is the temperature; μ_ω is the absorption coefficient for the laser radiation at a wavelength of 10.6 μm; k, U, and U_b are the absorption coefficient, medium radiation density, and black body radiation density; P_L is the laser beam power; subscript ω is used with spectral quantities; and subscript g is used with spectral group characteristics, which are derived by averaging over each of the N_g spectral ranges

$\Delta\omega_g$ in the total spectral region $\Delta\Omega$. The laser beam is taken as Gaussian, and R_b is the boundary of the laser beam.

The state equation is used in the following form:

$$\frac{p}{\rho} = \frac{R_0}{W_\Sigma} T \tag{9}$$

where R_0 is the universal gas constant, and W_Σ is the total molecular weight.

It is assumed that boundaries of the LSPG channel are absolutely black, and their temperature T_w is constant. The laser beam direction coincides with the x axis. At the input section of the channel ($x = 0$), an axial velocity is considered to be $u = u_0$. In the exit section, nonreflecting boundary conditions are used.

Because a laser-supported wave is caused by absorption of laser radiation in plasma at temperatures $\sim$15, 000–20, 000 K, a special Eq. (6) is formulated. An approximation of geometric optics is used for describing the laser radiation transfer.

The equation of radiation heat transfer is integrated in the form of a multigroup P_1 approximation of the spherical harmonics method [27]. For determination of radiation heat transfer characteristics (volume density of radiation energy and of radiation heat fluxes), it is necessary to integrate a system of N_g equations, Eq. (8). It should be stressed that the P_1 approximation was used only in the system of Eqs. (1–8) for predicting the radiative energy balance in the LSW. The P_1 approximation cannot be considered satisfactory for predicting the group radiation fluxes on internal surfaces, especially for optically thin media [27]. Therefore, another method, the ray-tracing method (RTM), was used to predict radiative heating of internal surfaces. The RTM algorithm is presented in this paper.

As mentioned here, the investigated process develops at approximately constant pressure that causes significant problems for a numerical solution of the task, because available disturbances of the pressure are hundreds of times less than background pressure. However, in this case, it is quite sufficient to take into account only the temperature dependencies of the thermophysical and optical properties that are included in the mathematical model (1–8). Temperature dependencies of the mentioned properties ρ, c_p, μ, λ, μ_ω, and κ_g were calculated only for the background pressure; for the main calculations, an interpolation procedure for temperature was used. The thermophysical and transport properties of a low temperature hydrogen plasma were used in a tabular form [25] (see Fig. 2).

Spectral and group (Fig. 3) absorption coefficients of hydrogen plasma were calculated using the computing program ASTEROID (absorption and selective transfer of electromagnetic radiation of ionized domains) [26]. The group optical model was created by averaging the spectral absorption coefficients over 37 spectral groups. This number of spectral groups was determined by performing numerical experiments with different numbers of spectral groups (from 2 up to 300). The concept of the choice of the acceptable number of spectral groups is discussed in [26,28,29]. There is a problem of optimization of the number: too low a number provides physically unrealistic results (for example, one can observe extinction of laser-supported waves for some calculation cases with low a number of spectral groups), whereas too large a number of the spectral groups results in large computational times. Therefore, from one side, the boundaries of the spectral groups (actually the spectral grid) must take into account the general peculiarity of the spectra of heat emissivity (processes of photo recombination, electronic bands of diatomic molecules, strong atomic lines, continuous radiation processes); from the other side, the spectral group model with a low number of spectral groups is favored over the spectral group model with a larger number of spectral groups. It was shown in the numerical experiments that the 37th-group model is quite acceptable for the problem under consideration. Just this group model was used for calculation of radiative gas dynamics and radiation fluxes on an internal surface of the LSPG.

As one can see from Figs. 2 and 3 all the mentioned thermophysical and optical parameters dramatically depend on temperature, pushing us to use detailed nonhomogeneous calculation grids to avoid significant errors in the interpolation of relevant properties.

From the computational fluid dynamics (CFD) point of view, this problem has some additional peculiarities. The first one is the low Mach number ($M \ll 1$), the second one is the existence of regions of drastic temperature drops (from 300 to $\sim$20, 000 K) and corresponding density drops, and the third one is the origination of self-oscillation of the gas flow inside and around the LSWs [22,30].

The CFD problem of subsonic gas flows with localized heat release regions was carefully studied in the literature. Specialized methods [11,12,18] were developed for numerical solutions of such tasks. A method of unsteady dynamical variables (UDV) [31,32], which is used in the present paper, was also developed especially for these purposes. The essence of the UDV method is the introduction of the traditional dynamic variables of the vorticity (ω) and the stream function (Ψ), and also a new additional function (ε) taking into account an inequality at zero for the derivative of a density with time:

$$\omega = \frac{\partial \rho v}{\partial x} - \frac{\partial \rho u}{\partial r}, \qquad \frac{\partial \Psi}{\partial y} = \exp(\varepsilon)\rho u, \qquad \frac{\partial \Psi}{\partial x} = -\exp(\varepsilon)\rho v \tag{10}$$

Equations (1–3) have the following form in these variables:

$$\frac{\partial \omega}{\partial t} + \operatorname{div}(\omega \boldsymbol{V}) + \frac{\partial}{\partial x}\left(\rho v \frac{\partial u}{\partial x} - \rho u \frac{\partial u}{\partial y}\right) + \frac{\partial}{\partial y}\left(\rho v \frac{\partial v}{\partial x} - \rho u \frac{\partial v}{\partial y}\right) = \frac{1}{Re}\left(\frac{\partial S_v}{\partial x} - \frac{\partial S_u}{\partial y}\right) \tag{11}$$

$$\operatorname{div}[\exp(-\varepsilon)\operatorname{grad}\Psi] = -\omega \tag{12}$$

$$\rho u \frac{\partial \varepsilon}{\partial x} + \rho v \frac{\partial \varepsilon}{\partial y} = \frac{\partial \rho}{\partial t} \tag{13}$$

where Re = Reynolds number and

$$S_u = \frac{4}{3}\frac{\partial}{\partial x}\left(\mu \frac{\partial u}{\partial x}\right) + \frac{1}{r}\frac{\partial}{\partial r}\left(r\mu \frac{\partial u}{\partial r}\right) + \frac{1}{r}\frac{\partial}{\partial r}\left(r\mu \frac{\partial v}{\partial x}\right) - \frac{2}{3r}\frac{\partial}{\partial x}\left(\mu \frac{\partial rv}{\partial r}\right)$$

$$S_v = \frac{\partial}{\partial x}\left(\mu \frac{\partial u}{\partial r}\right) + \frac{\partial}{\partial x}\left(\mu \frac{\partial v}{\partial x}\right) + \frac{4}{3r}\frac{\partial}{\partial r}\left(r\mu \frac{\partial v}{\partial r}\right) - 2\frac{\mu v}{r^2} - \frac{2}{3}\frac{1}{r}\frac{\partial}{\partial r}\left(r\mu \frac{\partial u}{\partial x}\right) - \frac{2}{3}\frac{1}{r}\frac{\partial \mu v}{\partial r} + \frac{2}{3}\frac{\mu}{r}\left(\frac{\partial u}{\partial x} + \frac{1}{2}\frac{\partial (rv)}{\partial r}\right)$$

The elimination of a pressure from the equations for subsonic gas dynamics noticeably simplifies the numerical simulation procedure for conditions of very small pressure differentials. An implicit numerical simulation method of second order in accuracy on spatial variables is used for integration of Eqs. (11–13). The five-point finite-difference scheme is realized by the successive overlapping method (SOR) with the Thomas algorithm along coordinate lines. Convergence of the numerical simulation algorithm was tested by quadrupling the computation grids.

As mentioned previously, flow oscillations were observed around the laser-supported waves [22,30]. Often, these oscillations play a positive role in the stabilization of the gas flow behind the LSW. Numerical study of the effect is presented in [33]. Following [33], an affective viscosity coefficient in the present study is calculated using the $k - \varepsilon$ model of turbulence.

III. Ray-Tracing Method for Prediction of Radiation Heat Fluxes on Internal Surface of the LSPG

The RTM was used to calculate the radiation heat fluxes to the surfaces of the LSPG. The problem geometry is shown in Fig. 1. The condition of axial symmetry is used in these calculations.

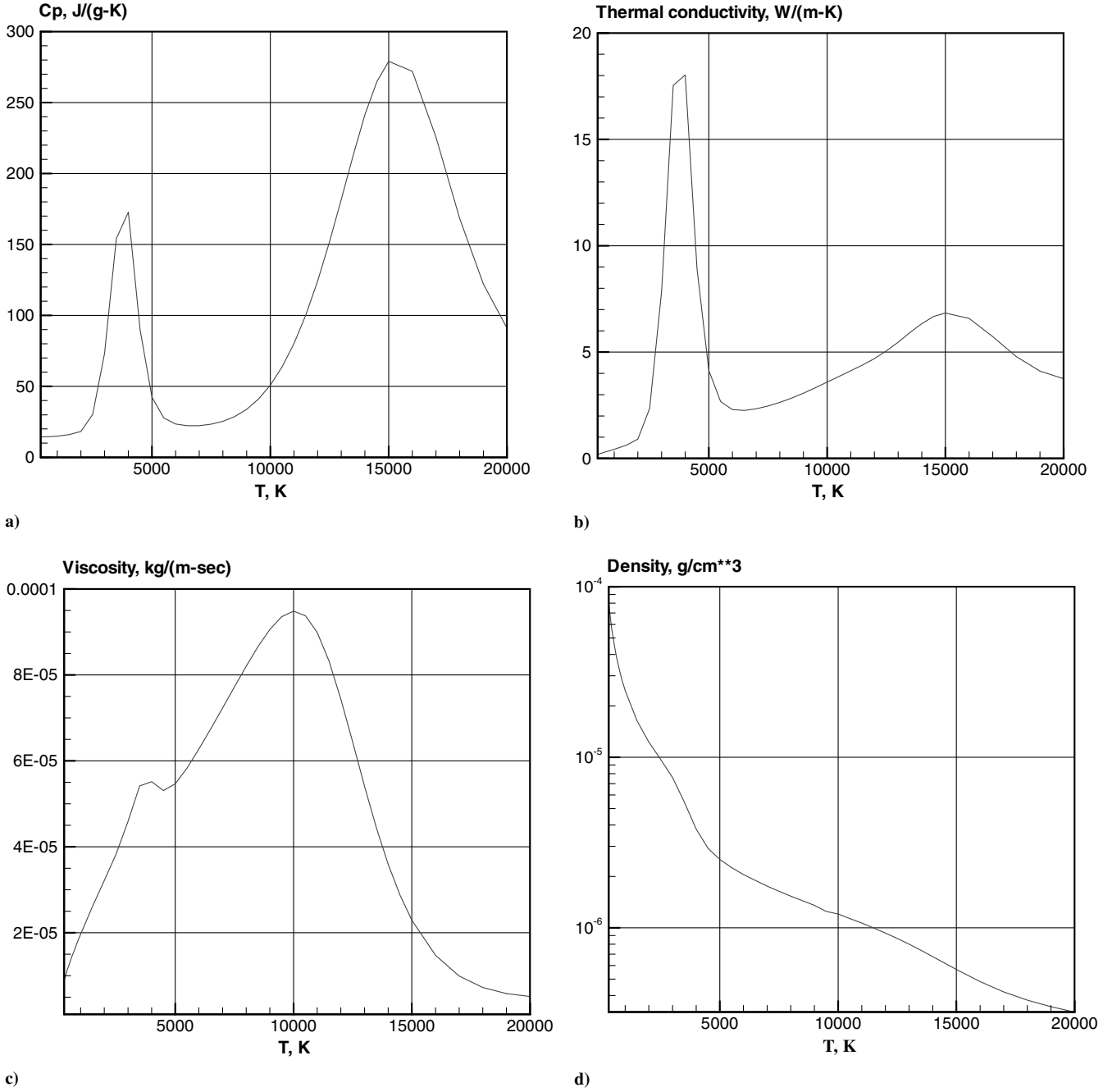

Fig. 2 a) Specific heat at constant pressure of hydrogen plasma at $p = 1$ atm. b) Total thermal conductivity of hydrogen plasma at $p = 1$ atm. c) Viscosity of hydrogen plasma at $p = 1$ atm. d) Density of hydrogen plasma at $p = 1$ atm.

An algorithm of the RTM consists of the following: To calculate the radiation heat flux to any element of the LSPG surfaces, it is necessary to enter the local spherical coordinate system, of which the z axis at each point coincides with the local normal to the internal LSPG surface. Then, the radiation heat transfer equation is integrated along each ray emitting from the point involved. Each ray $\boldsymbol{\Omega}$ is defined in this local coordinate system using the following two angular coordinates: the latitude angle $\theta \in [0, \pi/2]$, and the azimuth angle $\varphi \in [0, 2\pi]$.

The radiation heat flux is defined by the following equation:

$$W_v(\boldsymbol{R}_j) = \int_0^{2\pi} \mathrm{d}\varphi \int_0^{\pi/2} J_v(\boldsymbol{R}_j, \boldsymbol{\Omega}) \cos\theta \sin\theta \, \mathrm{d}\theta \qquad (14)$$

where $\boldsymbol{R}j(x_j, r_j)$ is the radius vector of the jth point on the LSPG surface in the laboratory coordinates system, x_j and r_j are the axial and radial coordinates of the jth point, and $J_v(\boldsymbol{R}_j, \boldsymbol{\Omega})$ is the spectral radiation intensity at the point R_j corresponding to direction $\boldsymbol{\Omega}$. The following grid was used for calculations:

$$\omega = \{h_i = r_i - r_{i-1} = \text{const}, h_j = x_j - x_{j-1} = \text{const}; i = 1, \ldots, NI, j = 1, \ldots, NJ\}$$

Introduction of a finite-difference mesh of angular directions allows us to integrate the spectral intensity in Eq. (14) in angular variables and to calculate the spectral radiation flux:

$$W_v(\boldsymbol{R}_j) = \sum_{m=1}^{N_\varphi - 1} (\varphi_{m+1} - \varphi_m) \sum_{n=1}^{N_\theta - 1} J_v(\boldsymbol{\Omega}) \tfrac{1}{2} (\sin\theta_{n+1} \cos\theta_{n+1} + \sin\theta_n \cos\theta_n)(\theta_{n+1} - \theta_n) \qquad (15)$$

or

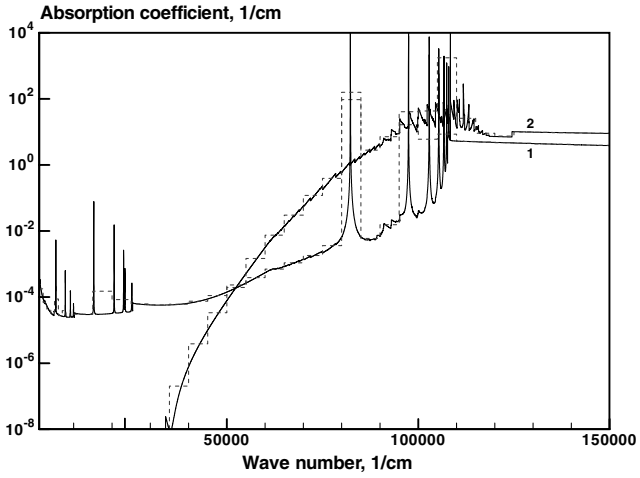

a)

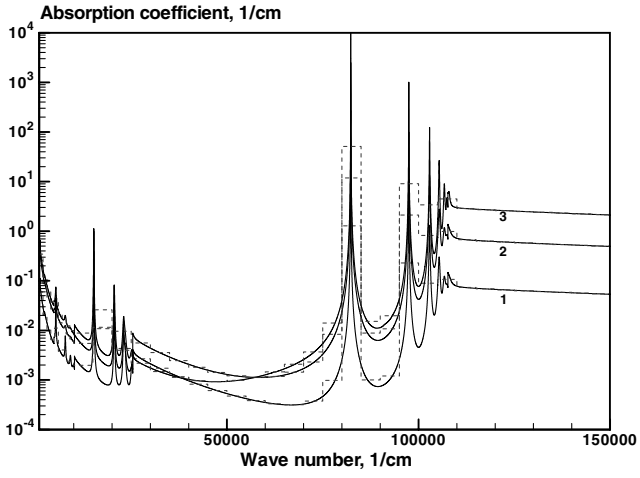

b)

Fig. 3 a) Spectral (solid line) and group absorption coefficients of a hydrogen plasma at $p = 1$ atm, $T = 8000$ K (1), and 4000 K (2). b) Spectral (solid line) and group absorption coefficients of a hydrogen plasma at $p = 1$ atm, $T = 20,000$ K (1), 16,000 K (2), and 12,000 K (3).

$$W_v(\boldsymbol{R}_j) = \sum_{m=1}^{N_\varphi - 1} (\varphi_{m+1} - \varphi_m) \sum_{n=1}^{N_\theta - 1} J_v(\boldsymbol{\Omega}_{m,n}) \frac{(\cos^2\theta_{n+1} - \cos^2\theta_n)}{2}$$

where N_φ is the number of rays on the azimuth angle and N_θ is the number of rays on the latitude angle. The direction cosines of the vector

$$\boldsymbol{\Omega}_{m,n} = (\omega_x)_{m,n}\boldsymbol{i} + (\omega_y)_{m,n}\boldsymbol{j} + (\omega_z)_{m,n}\boldsymbol{k}$$

are calculated by the following formulas:

$$(\omega_x)_{m,n} = \sin\theta_n \cos\varphi_m \quad (\omega_y)_{m,n} = \sin\theta_n \sin\varphi_m \quad (\omega_z)_{m,n} = \cos\theta_n$$

To calculate spectral radiation intensity, a radiation heat transfer equation should be integrated along the inhomogeneous optical path. The following solution of the radiation heat transfer equation can be used for this purpose:

$$J_v(\tau_v) = \int_0^{\tau_v} B_v(\tau'_v) \exp[-(\tau_v - \tau'_v)]\, \mathrm{d}\tau'_v \tag{16}$$

where $\tau_v = \int_0^s \kappa_v \, \mathrm{d}s'$ is the optical length; $B_v(T) = \frac{2hv^3}{c^2}[\exp(\frac{hv}{kT}) - 1]^{-1}$ is the black body radiation intensity; s is a coordinate along the ray, and $s = 0$ and $s = L$ are the initial (on the LSPG internal surface) and final (on the outer surface of the calculation region or on the LSPG conjugate surface) coordinates of the segment with directing vector $\boldsymbol{\Omega}_{m,n}$.

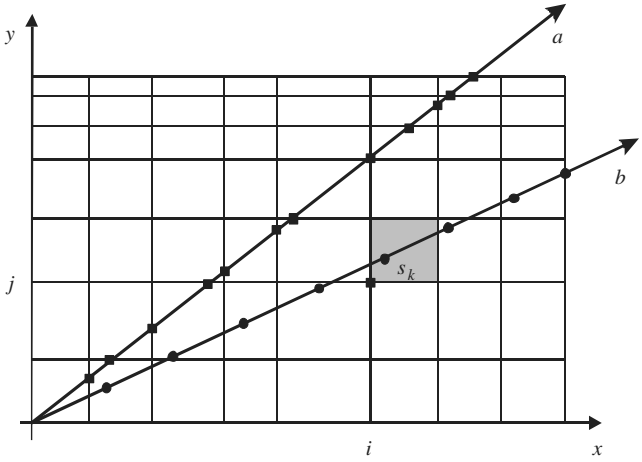

Fig. 4 Illustration of finite-difference scheme used for prediction of radiative heating on the external surface.

A finite-difference scheme for spatial variable s is formulated for each ray $\boldsymbol{\Omega}_{m,n}$. For this purpose, the coordinates of the intersections of the ray $\boldsymbol{\Omega}_{m,n}$ with all surfaces of the spatial finite-difference mesh should be calculated. This is illustrated in Fig. 4 (see points on ray *a*). Relations of the analytical geometry should be used for these purposes. However, this algorithm is not effective because of time-consuming calculations, especially for nonstructured meshes. A more effective algorithm of the quasirandom sampling was used in the present study. In the last case, a segment with direction vector $\boldsymbol{\Omega}_{m,n}$ (between the initial and final points) is divided on NS subregions as is shown in Fig. 4 (see points on the beam *b*). Then, the nearest node or elemental volume of a spatial computational grid is located for each node s_k. In that way, temperatures and spectral absorption coefficients are obtained for each node of the segment ($s = 0$ to $s = L$).

Numerical integration in Eq. (13) is realized as follows:

$$J(\tau_{NS}, \boldsymbol{\Omega}_{m,n}) = \exp(-\tau_{NS}) \left\{ \sum_{k=1}^{NS-1} \tilde{B}_k \exp(\tau_k)[\exp(\tau_{k+1} - \tau_k) - 1] \right\} \tag{17}$$

where

$$\tilde{B}_k = \frac{(B_k + B_{k+1})}{2}, \quad \tau_l = \sum_{i=1}^{l-1} \frac{(\kappa_i + \kappa_{i+1})}{2}(s_{i+1} - s_i), \quad l = 1, \ldots, NS$$

Note again that this calculating formula corresponds to a group approximation of the real spectrum. The accuracy of the approach is quite acceptable for prediction of radiative heating on internal surfaces. If there is a necessity to analyze the fine structure of the emission spectra (e.g., the atomic line structure), other spectral models can be recommended (e.g., line-by-line or random models).

Note that in the present case it is practically impossible to calculate radiative heating of the internal surface of LSPG channel by a P_1 method because the hydrogen plasma is optically thin in some spectral groups. At the same time, there are no principal limitations for using the P_1 approximation of the spherical harmonic method for numerical prediction of the volume density of radiation energy and the divergence of the group radiation heat flux. Therefore, two methods for solving the radiation heat transfer equations were used here. The ray-tracing method was used to predict radiative heating of internal surface, whereas the P_1 method was used to predict volume density of radiation energy. Estimation of the accuracy of the RTM method and its efficiency are presented in [29].

IV. Numerical Simulation Results

Radiative gas dynamics of a hydrogen laser plasma generator were studied for the following initial conditions: the power of CW CO_2

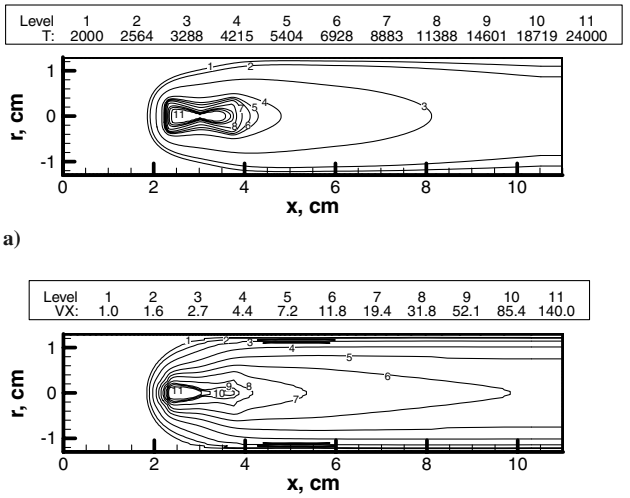

Fig. 5 Temperature (upper figure, T in K) and axial velocity (lower figure, $VX = u/u_0$) distributions in hydrogen LSPG. The volume emission approach with $u_0 = 2$ m/s is used.

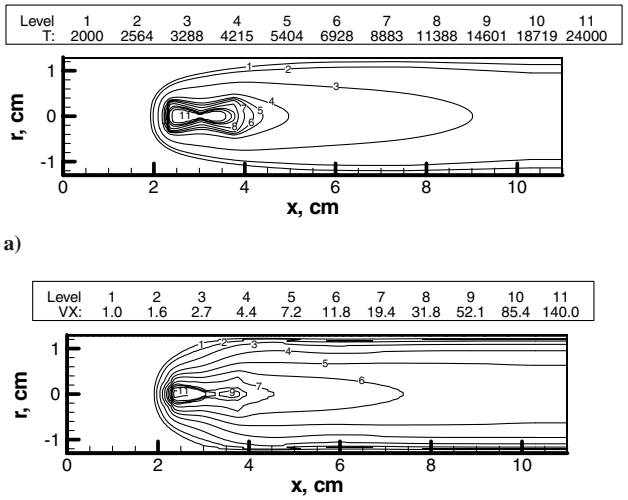

Fig. 6 Temperature (upper figure, T in K) and axial velocity (lower figure, $VX = u/u_0$) distributions in the LSPG. The volume emission approach with $u_0 = 5$ m/s is used.

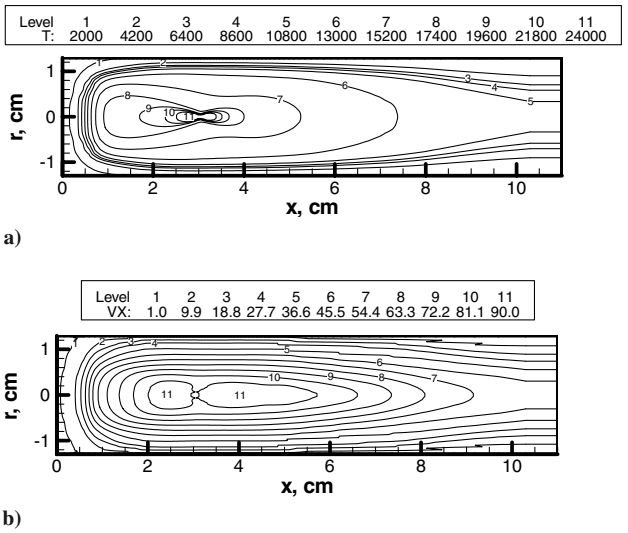

Fig. 7 Temperature (upper figure, T in K) and axial velocity (lower figure, $VX = u/u_0$) distributions in hydrogen LSPG. Full radiation heat transfer approach with $u_0 = 2$ m/s is used.

laser is $P_L = 200$ kW, the focal length of the focusing lens is $x_f = 3$ cm, the divergence of the laser radiation is $\theta = 0.1$ mradian, the initial radius of the laser beam is $R_b = 1.0$ cm, the pressure in the LSPG channel is $p_0 = 1$ atm, the gas velocities in the input section were changed in from $u_0 = 2$ to 60 m/s, and the lengths and radius of the LSPG channel are $L_c = 11$ cm and $R_c = 1.3$ cm.

The calculations were performed on succession nonhomogeneous finite-difference meshes with grid condensation around the high temperature zone of the LSW and near to the wall of the cylindrical channel. Numerical simulation results are presented for the following number of nodes along the axial and radial directions respectively: 60×30, 80×40, 120×50, and 240×100. A multiprocessor computer cluster was used for the calculations, which consisted of 16 Intel Pentium IV processors with a timing frequency for each processor of 3.2 GHz. A typical calculation time for one case was about 5–20 h.

Two series of calculations were performed. The first one was carried out for the radiation emission model (i.e., the optically thin approximation was used in this case, or the so-called volume emission approach). For an entrance velocity of $u_0 = 2$ m/s, the laser plasma moved toward the laser, and its forward front was fixed at a distance of $\sim$2.3 cm from the channel entrance (Fig. 5). In these cases, the distributions of all thermal and gas dynamic functions quickly stabilized and did not vary with time (i.e., the steady-state solution for the task was obtained). A temperature inside the LSW achieved $\sim$24, 500 K, but the plasma jet temperature was less than $\sim$3200 K. The temperature behavior inside the laser plasma can be explained by using the volume emission approach. Practically full absorption of the laser radiation by the plasma was obtained.

The next case studied was performed for the entrance velocity of $u_0 = 5$ m/s. Actually, this is an extreme velocity case at which the LSW can exist in a volume emission mode. A gas flow with $u_0 =$ 6 m/s blows off the LSW, and the laser plasma cannot exist as the numerical solution predicts. Figure 6 shows that, in this case, the high temperature plasma is more localized than in the previous case. In this case, the maximum temperature in the LSW is also about 24,000 K and the temperature in the laser plasma jet is about 3000 K.

The numerical simulation results show extremely high cooling of the laser plasma in the case of the volume emission approach. In this case, a configuration of the numerically calculated LSW follows the laser beam form near to its focusing point. It is worth noting that the volume emission approach predicts extinction of the LSW at low entrance velocities.

The second series of calculations was performed using the full radiation heat transfer model; that is, all radiation characteristics were calculated by solving the full system of Eq. (8) by using of the 37th group model. In this series, the entrance velocity was varied for significantly wide regions. Figures 7 and 8 show distributions of temperature and axial velocity for entrance velocities of $u_0 = 5$ and 50 m/s. Comparing data presented in Figs. 6–8, one can conclude that radiation heat transfer processes in the given type of LSPG are very significant, especially for the forming of the high temperature region and for prediction of the plasma jet velocity. For the full radiation heat transfer mode, the high temperature region of the LSW has a noticeably larger dimension. Its front is located at distance $\sim$1.5 cm from the entrance cross section of the LSPG channel for $u_0 = 5$ m/s. The greatest temperature inside the LSW runs up to $\sim$24, 000 K. This temperature is slightly smaller than that one obtained for the volume emission mode; but because of appreciably larger dimension of the heated region and because of reduction of total energy losses, the temperature of the plasma jet and its velocity are essentially larger. For $u_0 = 5$ m/s, the plasma jet temperature at the exit section of the LSPG channel reaches a value of 10,800 K, and the axial velocity is 250 m/s.

The maximal temperature in the plasma jet slightly decreases up to $\sim$9000 K at increasing of the entrance velocity (see Fig. 8). For maximum entrance velocity $u_0 = 50$ m/s, at which the LSW exists in the conditions under consideration, the plasma jet velocity

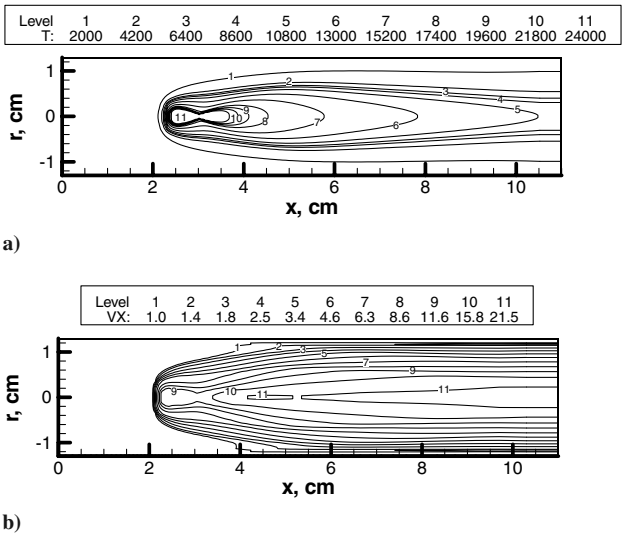

Fig. 8 Temperature (upper figure, T in K) and axial velocity (lower figure, VX $= u/u_0$) distributions in hydrogen LSPG. Full radiation heat transfer approach with $u_0 = 50$ m/s is used.

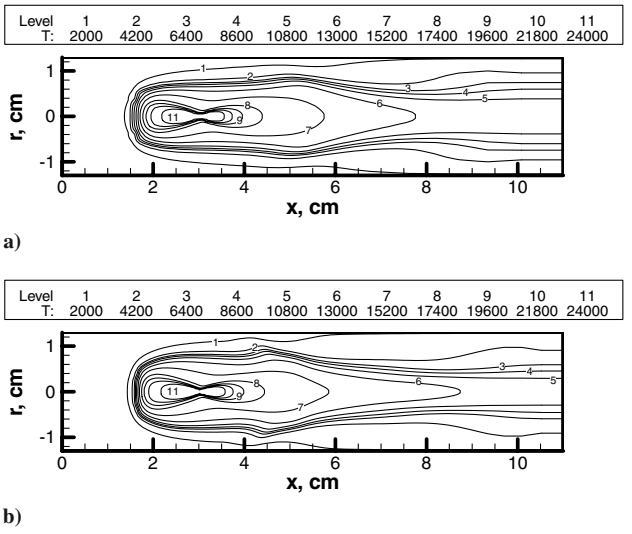

Fig. 9 Temperature (in K) distribution with an entrance velocity of 30 m/s; a) grid 60 × 30; b) grid 120 × 50.

achieves the value of 1075 m/s. At velocity $u_0 = 60$ m/s, the LSW is blown off by entrance hydrogen flow.

Results of methodical CFD study of the finite-difference method accuracy and of influence of spectral group models on numerical simulation results are shown in Figs. 9 and 10. Figure 9 shows two temperature fields obtained for two kinds of grids. As it was mentioned previously, to obtain a steady-state solution for the temperature field, the $k - \varepsilon$ turbulent model was used for prediction effective viscosity of gas flow inside the LSPG chamber. One can see that a variation of calculation grids in wide region results in some changing of temperature profiles, but the general peculiarities of the thermal structure of LSW were left unchanged.

Figure 10 shows temperature fields for different spectral group optical models. It is worth noting that the spectral group model has a large influence on the temperature distribution for the calculation cases when the heat radiation plays a dominant role in the energy balance inside the laser-supported waves. Two spectral group models ($N_g = 37$ and 77) provide acceptable agreement between numerical simulation results. At a lower number of spectral groups, large differences were observed in the temperature fields. Sometimes, low group optical models result in the extinction of the LSW.

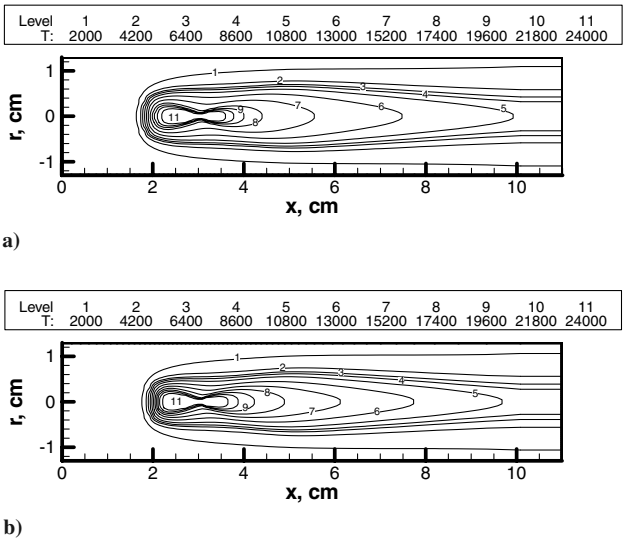

Fig. 10 Temperature (in K) distribution with an entrance velocity of 40 m/s; a) $N_g = 37$; b) $N_g = 77$.

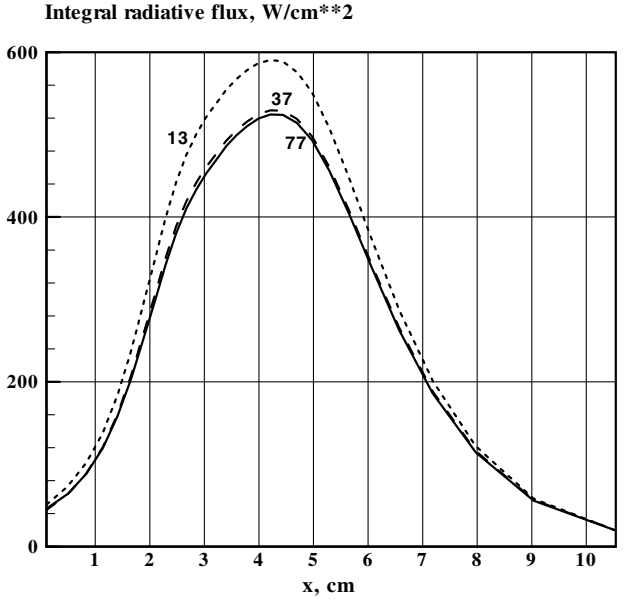

Fig. 11 Integral radiation heat flux along internal cylindrical surface of the hydrogen LSPG for different spectral group models (numbers near to the curves designate number of spectral groups).

Calculations of radiative heating of the internal surface of a LSPG were performed for each calculation case. The ray-tracing method was used with an angular mesh of $N_\theta = N_\varphi = 21$ and $NS = 20$ [see Eq. (15)]. Our calculations have confirmed that the radiative heat fluxes predicted by the RTM strongly depend on the parameters of the spatial finite-difference mesh. Numerical simulation results presented in Figs. 11–13 correspond to the minimal acceptable mesh. The angular mesh was established with numerical experiments in which the number of nodes in each angular direction was varied over a wide region (10–100). Figure 11 illustrates the dependence of the integral radiation flux distribution on the internal surface obtained by using different numbers of spectral groups. One can see that there is satisfactory convergence of the radiation flux distributions depending on the number of spectral groups. Not only is the number of spectral groups important but also the wave number distribution on the spectral grid. Figure 12 shows the spectral grids used in this work. This figure presents spectral group radiation heat fluxes at two axial points along the internal surface of the LSPG chamber at $x = 0$ and at $x = 3.6$ cm. The spectral distribution shows that the

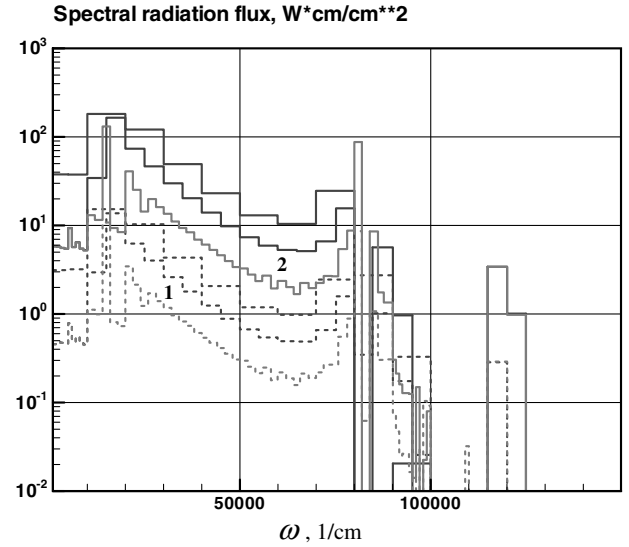

Fig. 12 Spectral group heat flux at $x = 0$ (1), and $x = 3.6$ cm (2) for $N_g = 13$, 37, and 77 groups.

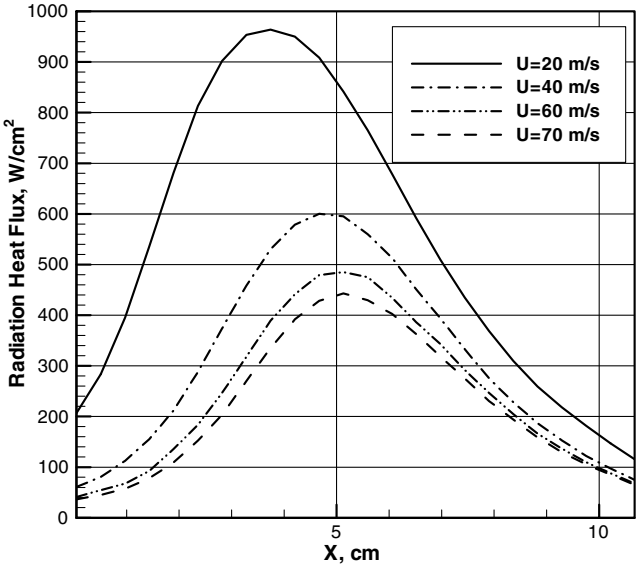

Fig. 13 Integral radiation heat flux along internal cylindrical surface of the hydrogen LSPG, W/cm^2, at different entrance velocities. The ray-tracing method is used.

maximum radiative heating lies in the range of the visible spectrum around $\sim 20,000$ cm^{-1}.

The tendency of decreasing radiative heating of the internal surface with increasing of the entrance velocity is demonstrated in Fig. 13. The high temperature region of the LSW in the plasma generator channel, as well as the relatively low temperature region, becomes smaller for increasing entrance velocities. One can also see that the region of heated gas is constricted (compare, for example, Figs. 7 and 8). These two facts lead to a decrease of the radiative heating of the internal surface. The numerical simulation results were also obtained for a power of the CW CO_2 laser of $P_L = 100$ kW and a radius of the LSPG channel of $R_c = 2.0$ cm. Temperature distributions were obtained by solving the radiative gas dynamic (RadGD) model, Eqs. (1–8), at values of entrance velocities of hydrogen flow of $u_0 = 20$–70 m/s. Note that for the larger channel radii, the laser-supported wave exists for higher input velocities. This can be explained by the larger mass flow, which is blowing out through the region of higher temperature of the laser-supported wave in the case of a decreased radius of the channel. It is obvious that, in this case, the conditions of the laser plasma cooling are much better. Therefore, the limit of the existence of the laser plasma in variables of laser power and input velocity is shifted in the direction of smaller velocities.

V. Conclusions

A radiative gas dynamic (RadGD) model of the laser-supported plasma generator (LSPG) with a hydrogen actuating fluid is developed and presented. This RadGD model is based on the system of the Navier–Stokes equations, an energy conservation equation, and heat and laser radiation transfer. A detailed description of the thermophysic, transport, and spectral optical properties of hydrogen plasma is used in this model. Two numerical simulation methods have been applied for prediction of the radiation heat transfer inside a LSPG channel. The ray-tracing method was used for calculation of the radiation heat fluxes on the internal surface of the LSPG, whereas the P_1 approximation of the spherical harmonic method was used for coupled radiative gas dynamic calculations.

The developed model is applied to the study of the hydrogen LSPG functioning in the radiative mode (i.e., when there are two general mechanisms of energy exchange: absorption of laser radiation in hydrogen plasma and radiation heat transfer of the high temperature plasma region with the ambient gas).

A numerical study has been performed for regimes of strong radiative-convection interaction. It has been shown that the distribution of the thermic and gas dynamic parameters is generally formed by the heat radiation transfer.

Acknowledgments

This work has been supported by PRIN Contract No. 2004-092040-003, Bari University Contract No. 63396 III/11, and by the Russian foundation for basic research Grant No. 05-01-00780. The authors thank J. Menart for valuable discussions.

References

[1] Raizer, Yu. P., and Surzhikov, S. T., "Continuous Laser Sustained Plasma and Laser Sustained Combustion; State of the Art," AIAA Paper 95-1999, 1995.

[2] Glumb, R. J., and Krier, H., "Concepts and Status of Laser-Supported Rocket Propulsion," *Journal of Spacecraft and Rockets*, Vol. 21, No. 1, 1984, pp. 70–79.

[3] Jones, L. W., and Keefer, D. R., "NASA's Laser-Propulsion Project," *AIAA Journal*, Vol. 20, No. 9, 1982, pp. 66–73.

[4] Black, J., Krier, H., and Glumb, R. J., "Laser Propulsion 10-kW Thruster Test Program Results," *Journal of Propulsion and Power*, Vol. 11, No. 6, 1995, pp. 1307–1316.

[5] McCay, T. D., Eskrige, R. H., and VanZandt, D. H., "Experiments on Optical Discharges in Hydrogen," *Journal of Thermophysics and Heat Transfer*, Vol. 2, No. 4, 1988, pp. 317–323.

[6] Klosterman, E. L., and Byron, S. R., "Measurement of Subsonic Laser Absorption Wave Propagation Characteristics at 10.6 μm," *Journal of Applied Physics*, Vol. 45, No. 11, 1974, pp. 4751–4759. doi:10.1063/1.1663130

[7] Conrad, R., Raizer, Yu. P., and Surzhikov, S. T., "Continuous Optical Discharge Stabilized by Gas Flow in a Weakly Focused Laser Beam," *AIAA Journal*, Vol. 34, No. 8, 1996, pp. 1584–1588.

[8] Metrogul, A. E., and Krier, H., "Two-Temperature Modeling of Laser Sustained Hydrogen Plasma," *Journal of Thermophysics and Heat Transfer*, Vol. 8, No. 4, 1994, pp. 781–790.

[9] Metrogul, A. E., Zerkle, D., and Krier, H., "Investigation of CO_2 Laser Sustained Hydrogen Plasmas," *Journal of Propulsion and Power*, Vol. 8, No. 5, 1992, pp. 1123–1125.

[10] Jeng, S. M., and Keefer, D. R., "Numerical Study of Laser Sustained Hydrogen Plasmas in a Forced Convective Flow," *Journal of Propulsion and Power*, Vol. 3, No. 3, 1987, pp. 255–261.

[11] Merkle, C. L., "Prediction of the Flowfield in Laser Propulsion Devices," *AIAA Journal*, Vol. 22, No. 8, 1984, pp. 1101–1107.

[12] Molvik, G. A., Choi, Y.-H., and Merkle, C. L., "A Two-Dimensional Analysis of Laser Heat Addition in a Constant Absorbing Gas," *AIAA Journal*, Vol. 23, No. 7, 1985, pp. 1053–1060.

[13] Jackson, J. P., and Nielsen, P. E., "Role of Radiative Transport in the Propagation of Laser Supported Combustion Waves," *AIAA Journal*, Vol. 12, No. 11, 1974, pp. 1498–1501.

[14] Keefer, D. R., Peters, C. E., and Crowder, H. L., "A Reexamination of the Laser Supported Combustion Wave," *AIAA Journal*, Vol. 23, No. 8, 1985, pp. 1208–1212.

[15] Glumb, R. J., and Krier, H., "Two-Dimensional Model of Laser-Sustained Plasmas in Axisymmetric Flowfields," *AIAA Journal*, Vol. 24, No. 8, 1986, pp. 1331–1336.

[16] Zerkle, D. K., and Krier, H., "Nonlocal Thermodynamic Equilibrium in Laser-Sustained Plasmas," *AIAA Journal*, Vol. 32, No. 2, 1994, pp. 324–332.

[17] Raizer Yu. P., and Surzhikov, S. T., "Investigation of the Processes Occurring in an Optical Plasmatron by Numerical Calculation," *Soviet Journal of Quantum Electronics*, Vol. 14, No. 11, 1984, pp. 1526–1535.
doi:10.1070/QE1984v014n11ABEH006484

[18] Surzhikov, S. T., "Numerical Simulation of Slow Steady Combustion in a CO_2 Laser Beam," *Mathematical Modeling and Computing Experiment*, Vol. 1, No. 4, 1993, pp. 355–365.

[19] Surzhikov, S. T., "Radiative Convective Heat Transfer in an Optical Plasmatron Chamber," *High Temperature*, Vol. 28, No. 6, 1990, pp. 926–932.

[20] Generalov, N. A., Zaharov, A. M., Kosynkin, V. D., and Yakimov, M. Yu., "Stability of the Optical Discharge in Atmospheric Air Flow," *Combustion, Explosion, and Shock Waves*, Vol. 22, No. 2, 1986, pp. 214–218.
doi:10.1007/BF00749269

[21] Surzhikov, S. T., "Numerical Analysis of Subsonic Laser Supported Combustion Waves," *Quantum Electronics*, Vol. 30, No. 5, 2000, pp. 416–420.
doi:10.1070/QE2000v030n05ABEH001720

[22] Surzhikov, S. T., and Chentsov, A. A., "Numerical Study of the Stability of Optical Discharges in Air Flow," *Plasma Physics Reports*, Vol. 22, No. 11, 1996, pp. 957–963.

[23] Raizer, Yu. P., and Surzhikov, S. T., "Thermo-Gravitational Convection in a Continuous Optical Discharge," *Fluid Dynamics*, No. 4, 1989, pp. 593–598.

[24] Uhlenbusch, J., "High Pressure Continuous Optical Discharge," *Proceedings of the XVI International Conference on Phenomena in Ionized Gases*, edited by W. Bötticher, H. Wenk, and E. Schultz-Guldeed, Dusseldorf Univ., Dusseldorf, Germany, 1983, pp. 119–130.

[25] Capitelli, M., Colonna, G., Gorse, C., Minelli, P., Pagano, D., and Giordano, D., "Thermodynamic and Transport Properties of Two Temperature H_2 Plasmas," AIAA Paper 2001-3018, 2001.

[26] Surzhikov, S. T., "Computing System for Mathematical Simulation of Selective Radiation Transfer," AIAA Paper 2000-2369, 2000.

[27] Devison, B., and Sykes, J. B., *Neutron Transport Theory*, Oxford Univ. Press, New York, 1957.

[28] Surzhikov, S., Capitelli, M., and Colonna, G., "Spectral Optical Properties of Nonequilibrium Hydrogen Plasma for Radiation Heat Transfer," AIAA Paper 2002-3222, 2002.

[29] Filipskiy, M. V., and Surzhikov, S. T., "Discrete-Ordinates Method for Prediction of Radiative Heating of Space Vehicles," AIAA Paper 05-4948, 2005.

[30] Surzhikov, S. T., "Bifurcation of Subsonic Gas Flows in the Vicinity of Localized Heat Release Regions," arXiv:physics [online], e-print service from Cornell University, http://arxiv.org/abs/physics/0605033v2 [retrieved 4 May 2006].

[31] Surzhikov, S. T., "Numerical Simulation Method for Slow Unsteady Flows Near to Local Heat Release Regions," AIAA Paper 98-2829, June 1998.

[32] Surzhikov, S. T., and Krier, H., "Unsteady Dynamic Variables Method for Heterogeneous Solid Propellant Burning," *AIAA Journal*, Vol. 39, No. 12, 2001, pp. 2343–2350.

[33] Surzhikov, S. T., "Laser-Plasma Generator with Artificial Turbulence of the Input Gas Stream," *Journal of Thermophysics and Heat Transfer*, Vol. 15, No. 2, 2001, pp. 239–242.